Statistical Survey of Interchange Events in the Jovian Magnetosphere Using Juno Observations

A. Daly[1], W. Li[1], Q. Ma[1,2], X.-C. Shen[1], L. Capannolo[1], S. Huang[1], W. S. Kurth[3], G. B. Hospodarsky[3], B. H. Mauk[4], G. Clark[4], F. Allegrini[5,6], and S. J. Bolton[5]

[1]Center for Space Physics, Boston University, Boston, MA, USA.

[2]Department of Atmospheric and Oceanic Sciences, University of California, Los Angeles, CA, USA.

[3]Department of Physics and Astronomy, University of Iowa, Iowa City, IA, USA.

[4]The Johns Hopkins University Applied Physics Laboratory, Laurel, Maryland, USA.

[5]Southwest Research Institute, San Antonio, Texas, USA.

[6]University of Texas at San Antonio, San Antonio, Texas, USA.

Corresponding authors: Alec Daly (adaly@bu.edu); Wen Li (wenli77@bu.edu)

Key Points:

- Our statistical survey indicates that interchange events occur over L (or *M*)-shells~6-26 at Jupiter with a peak occurrence rate at *M*~17.
- During interchange events, various types of plasma waves are intensified, each exhibiting a distinct preferential location.
- The duration and the corresponding spatial extent of interchange events are analyzed for multiple events.

Abstract

Interchange instability is known to drive fast radial transport of electrons and ions in Jupiter's inner and middle magnetosphere. In this study, we conduct a statistical survey to evaluate the properties of energetic particles and plasma waves during interchange events using Juno data from 2016 to 2023. We present representative examples of interchange events followed by a statistical analysis of the spatial distribution, duration and spatial extent. Our survey indicates that interchange instability is predominant at *M*-shells from 6 to 26, peaking near 17 with an average duration of minutes and a corresponding *M*-shell width of <~0.05. During interchange events, the associated plasma waves, such as whistler-mode, Z-mode, and electron cyclotron harmonic waves exhibit a distinct preferential location. These findings provide valuable insights into particle transport and the source region of plasma waves in the Jovian magnetosphere, as well as in other magnetized planets within and beyond our solar system.

Plain Language Summary

The radial transport of plasma around a magnetized planet is crucial for understanding the underlying magnetospheric dynamics. Jupiter's magnetospheric dynamics are primarily dominated by the rapid rotation and plasma source from Io. This rapid rotation drives the

interchange instability, where hot, low-density plasma is moved towards the inner magnetosphere. During this process, the inward moving flux tube builds up magnetic pressure, potentially leading to the trapping of particles alongside plasma waves. In this study, we present several typical examples of interchange events, and conduct a statistical analysis to explore their spatial distribution, duration and spatial extent, as well as the typical features of the associated plasma waves. This survey provides insights into mass transport, the source of these plasma waves in Jupiter's magnetosphere, with potential implications for other magnetized planets within and beyond our solar system.

1 Introduction

Interchange instability can occur through a local gradient in flux tube content, driven by centrifugal force from a rapidly rotating magnetosphere (Southwood & Kivelson 1987, 1989; Thomsen, 2013). This instability plays an important role in mass and plasma transport in Jupiter's magnetosphere, driving magnetic flux tubes containing cold dense plasma in the inner magnetosphere to interchange with more distant flux tubes of hot tenuous plasma (Bagenal et al., 2011; Dumont et al., 2014). Modeling demonstrates that this instability influences the radial transport of plasma from 10-20 R_J (Jupiter Radii) and affects the magnetopause standoff distance (Feng et al., 2023; Tanaka et al., 2023). This instability also occurs at Saturn and has the potential to occur in planetary systems beyond our solar system (Tilley et al., 2016). Interchange "injections" can be distinguished from large-scale transport related to reconnection processes in the magnetotail based on event location or the instability's driving mechanism (Mitchell et al., 2015; Azari, 2020).

The Galileo spacecraft first observed interchange at Jupiter in 1997. The spacecraft detected flux tubes characterized by low mass content, whistler-mode wave intensification, a rapid increase in magnetic field strength, and an enhancement of electron flux from 15 to 300 keV (Bolton et al., 1997; Kivelson et al., 1997; Thorne et al., 1997). Sharp gradients in magnetic field strength at the edge of the flux tube are associated with variations in plasma pressure and are expected to influence local energetic particle drifts (André et al., 2005, 2007; Lai et al., 2016). The drifts of these bouncing particles can be used to estimate the age, speed, and source region of interchange events (Burch et al., 2005; Hill et al., 2005; Paranicas et al., 2020; Rymer et al., 2009; Yin et al., 2023).

Recent studies at Jupiter identified interchange injections associated with Electron Cyclotron Harmonic (ECH), whistler-mode, and Z-mode waves (Daly et al., 2023; Kurth et al., 2023). ECH waves are observed between the harmonics of the electron gyrofrequency (f_{ce}), with their excitation mechanism attributed to the loss-cone instability of hot plasmas in the presence of cold background plasmas, often satisfied in injection regions (Ashour-Abdalla & Kennel, 1978; Horne et al., 2003; Kennel et al., 1970; Zhang & Angelopoulos, 2014). Joseph et al. (2023) found that ECH waves occur near the Io torus (associated with interchange injections) or the equatorial region of the middle magnetosphere. Whistler-mode waves are electromagnetic emissions between the electron and proton gyrofrequencies, generated near the equator from an anisotropic distribution of plasma sheet electrons (Hospodarsky et al., 2012; Kennel, 1966; Li et al., 2008). These waves have been observed from the equator to high magnetic latitudes over M-shells of 6-13 (Li et al., 2020; Menietti et al., 2021), where M-shell is defined as the radial distance from the equatorial crossing of a magnetic field line to the center of Jupiter in Jovian radii. Z-mode waves are electromagnetic emissions confined between the left-hand cutoff frequency and the upper hybrid frequency, likely generated through the electron cyclotron maser instability (Wu & Lee, 1979; Yoon et al., 1998). Z-mode waves are typically observed near the polar region (Kasier et al., 1993) and at middle latitudes at *M*-shell<~10 (Menietti et al., 2021), with a possible source near the outer and inner edges of the Io torus (Menietti et al., 2023). During interchange events, the modified distributions of electrons are highly anisotropic, thus are conductive to wave growth (Daly et al., 2023). Such wave growth can induce electron pitch angle scattering and precipitation through resonant interactions (e.g., Bhattacharya et al., 2005; Horne & Thorne, 1998; Li et al., 2021, 2023; Ni et al., 2012; Xiao et al., 2003).

While individual interchange events have been reported at Jupiter, a systematic survey on their occurrence and associated wave and particle properties remains limited. In the present study, we conduct a statistical analysis of interchange events using Juno data (Bolton, 2010) to determine their occurrence rate, spatial location, duration, instability source region, and properties of associated plasma waves, including ECH, whistler-mode, and Z-mode waves.

2 Juno Data and Event Selection

Juno's instruments, which measure particles, plasma waves, and magnetic fields, are crucial for analyzing the characteristics of energetic particles and plasma waves during interchange events. We use data from the Waves instrument (Kurth et al., 2017) to analyze plasma wave properties. To identify relevant wave modes, cyclotron frequencies are calculated based on in situ magnetic field measurements from the Magnetic Field Investigation instrument (Connerney et al., 2017). Particle data are collected by the Jovian Auroral Distributions Experiment (JADE) instrument (McComas et al., 2017) for ~50 eV–100 keV electrons and the Jupiter Energetic Particle Detector Instrument (JEDI) for ~25 keV–1 MeV electrons (Mauk et al., 2017).

Interchange events are identified based on electron fluxes measured by JADE and JEDI and magnetic field measurements at 3<*M*<30. Detailed identification methods are presented in Supporting Information Text S1. These criteria identified 87 clear interchange events. It is worth noting that conditions for magnetically depressed flux tubes were also explored, but no clear events were identified, in contrast to findings at Saturn (Lai et al., 2016). To enrich the dataset and identify potential events that may have been missed due to possibly restrictive criteria, we developed a deep neural network classifier (detailed in Text S2). The 87 events were used to create training, test, and validation datasets for a fully connected neural network model which learns the patterns in the events and identifies interchange events beyond those described in Text S1. By using this approach, 20 additional events were identified. The analysis presented in this study includes all 107 interchange events. This dataset is not unique or complete and depends on the model and the original 87 events used for training.

3 Statistical Results

3.1 Juno Observation of Interchange Events

Figure 1 illustrates three examples of interchange events, each associated with a different type of plasma wave. Particle and wave measurements were recorded for the first event on 06 September 2018 (perijove 15 or PJ-15), revealing two events over 19:10:20-19:11:13 UT and

19:13:27-19:14:22 UT, referred to as interval 1 and interval 2 henceforth. Both events were observed alongside Z-mode wave intensification at *M*-shell~9.6, magnetic latitude (MLat)~20.8°, and magnetic local time (MLT) of 1.6h. Interval 1 includes two closely spaced events, indicated by changes in magnetic field strength and electron flux (Figures 1a, b), which are treated as a single event due to their proximity. During these events, the magnetometer detected rapid changes in magnetic field strength (dB/dt) of 0.94 and 0.75 nT/s at the start of the first and second intervals, and -1.0 and -0.80 nT/s at the end of each interval (Figure 1a). The JEDI instrument observed a rapid increase in electron flux along with a slight energy dispersion likely due to gradient and curvature drifts (Figure 1b). The JADE instrument also detected variations in electron flux (Figure 1c), albeit less prominently compared to the JEDI measurements, possibly owing to the lower time resolution of the instrument during this interval. The JEDI instrument revealed increases in electron flux at 33 keV (Figure 1e) while the change is unclear from JADE at 90 eV (Figures 1d). During both events, electric wave emissions, identified as Z-mode waves, were detected with the lower cutoff at the left-hand cutoff frequency ($f_{L=0}$) and the upper cutoff below the plasma frequency (f_{pe}), as expected for left-hand polarized Z-mode waves (Figures 1f, g). The modeled plasma frequency (f_{pe_m}), derived from the empirical 2D density model (Dougherty et al., 2017), is included for intervals outside the event. Intensifications outside of the event between f_{ce} and $2f_{ce}$ are likely ECH waves (Figure 1f), which disappeared inside of the event, possibly due to changes in hot and cold electron density (Ashour-Abdalla and Kennel, 1978; Joseph et al., 2023). Based on $\boldsymbol{f_{pe} \approx 8980\sqrt{n_e}}$ Hz, the density (n_e) inside intervals 1 and 2 is approximately 1.15 cm^{-3}, compared to the modeled density outside the event (~15 cm^{-3}), indicative of an inward moving flux tube (Bolton et al., 1997).

The second example of two interchange events is associated with whistler-mode wave intensifications. These events were recorded on 16 October 2021 (PJ-37), spanning 02:27:27-02:30:05 and 02:30:59-02:33:20 UT. These events occurred at *M*~16.7, MLat~-10°, and MLT~1.4h. Within these events, the JEDI instrument detected a rapid increase in electron flux (Figure 1i), while the JADE instrument revealed a rapid decrease in electron flux (Figure 1j). The pitch angle distribution of both high and low energy electrons appears nearly isotropic both inside and outside the event (Figure 1k, l). The intensification of wave electric spectral density below f_{ce} is likely attributed to oblique whistler-mode chorus waves (Figure 1m), as no appreciable wave power was detected in the magnetic spectral density (Figure 1n).

The final interchange event example is associated with ECH waves. This period also reveals two close interchange events on 15 April 2021 (PJ-33) at *M*~15.2, MLat~-1°, and MLT~21.4h, occurring over 08:18:05-08:19:25 and 08:20:09-08:21:22 UT. Similar to previous examples, high-energy electrons exhibit a slight enhancement in flux (Figure 1p), while the low-energy electrons demonstrate a rapid dropout in flux (Figure 1q). The resultant pitch angle distribution of electrons at 33 keV is primarily field aligned (Figure 1s), while the 45 eV electrons are nearly isotropic (Figure 1r). While there is no noticeable wave magnetic intensification (Figure 1u), ECH waves are intensified within the interchange events (Figure 1t). The first interval exhibits intensifications in the first three harmonics of f_{ce}, while the second interval primarily shows an intensification in the first harmonic.

Each of these interchange events are indicative of inward radial transport, which is suggested by the total electron density decrease inferred from the f_{pe} during the Z-mode event or calculated from the JADE flux during the whistler-mode and ECH associated events. Additional interchange events detected by Juno can be found in Daly et al. (2023), Kurth et al. (2023), or in the data availability statement.

3.2 Distribution of interchange events in M, MLat, and MLT

We evaluated the distribution of interchange events from PJ 01 to PJ 51 spanning July 2016 to May 2023. Figure 2 shows the distributions of these events in *M*-shell, MLat, and MLT, along with associated plasma waves within the events. In Figure 2a, we examine the interchange events in *M*-shell versus MLat domain, where events associated with Z-mode waves are marked as orange triangles, whistler-mode waves as red squares, ECH waves as green diamonds, and events with no plasma waves as open black circles. The count rate or the number of identified interchange events is shown for both *M*-shell (bin size of 2) over $6<M<26$, and MLat (bin size of 5°) over -20°<MLat<45°. Our observations include 107 distinct interchange events, with a peak count rate occurring near $M\sim17.5$ within 5° of the magnetic equator. These observations align with previous models (e.g., Tanaka et al., 2023) at Jupiter, where interchange instabilities dominate over 15-20 R_J and also play a role over 10-15 R_J. Further information regarding the occurrence rate of these interchange events is provided in Supporting Information Figure S1.

Z-mode wave-associated interchange events were observed as two groups across *M*-shells ranging from 6.6-25.7 in the mid-latitudes (MLats of 17.1-42°), as illustrated in Figure 2a. The first group occurred within $6<M<10$, consistent with the inferred source region of Z-mode waves being the outer edge of the Io torus, as well as observations of Z-mode waves above 20° beyond 6 R_J (Menietti et al., 2023). It is noteworthy that the second group of Z-mode wave associated interchange events is distributed across *M*-shells of 18 to 26 at higher latitudes (>30°).

Whistler-mode wave-associated interchange events are observed across $M\sim8.7$-22.4 and MLats of -15.8-17.1°. These observations agree with previous surveys on whistler-mode waves, which indicate their preferential occurrence at |MLat|<50° across *M*-shells of 6 to 20, particularly for whistler-mode chorus waves within |MLat|<30° (Li et al., 2020; Menietti et al., 2023). The source region of these waves is believed to be outside Io's orbit and near the magnetic equator (Menietti et al., 2023).

The interchange events associated with ECH waves are observed across *M*-shells from 8.7 to 17.3 and MLats from -3.8 to 15.3°. The majority of these ECH waves are distributed near the equatorial region (|MLat|<5°), while some ECH waves are distributed at higher latitudes (>10°). This distribution pattern agrees with recent observations of ECH waves at Jupiter (Joseph et al., 2023), where ECH waves were intensified near the Io torus associated with interchange injections, characterized by $f_{pe}>f_{ce}$, and also observed alongside the magnetic equator in the middle magnetosphere.

It is notable that in some interchange events, no plasma wave intensification is observed, likely due to unfavorable plasma conditions inhibiting wave growth. The distribution of such interchange events without changes in plasma waves ranges from *M*-shells of 8.7-22.5 and |MLat| up to 20°, as marked by black circles in Figure 2a.

Figure 2b shows the M-MLT distribution of the corresponding interchange events by merging events from all magnetic latitudes. Juno provided good coverage over the nightside from 2016 to 2023, while dayside coverage was limited. Z-mode wave-associated interchange events preferentially occur in the postmidnight sector, while ECH wave-associated interchange events tend to occur in the premidnight sector. However, whistler wave-associated events occur in both the premidnight and postmidnight sectors. It is noteworthy that the MLT-dependence of these events remains inconclusive due to the limited coverage and the limited number of events in each MLT sector.

3.3 Duration and Spatial Extent

We analyze the duration of the interchange events and the corresponding widths in *M*-shell (ΔM) of the spacecraft crossing the interchanged flux tube. The duration and ΔM of the first interchange intervals are indicated as blue text on the top panel of Figure 1 for the three examples. The reported values for the duration and ΔM may represent the minimum estimates, due to the challenge of precise measurements from a moving spacecraft.

Figure 3 illustrates the duration and ΔM for all identified interchange events. The scatterplot in the *M*-shell versus MLat domain (Figure 3a) indicates that the average duration at lower *M*-shells (<15) is relatively short, with an average value of ~1.1 minutes, while the average duration at *M*-shells from 15 to 26 is ~2.1 minutes. These results imply that events beyond M=15 may last longer and/or have larger spatial extent, as estimated under the assumption of rigid corotation. Similar observations of larger-scale interchange events at greater distances have been reported at Saturn (Azari et al., 2018; Chen et al., 2010). The MLT dependence of the duration (Figure 3b) is unclear, with the longest event observed over 3-6 MLT.

Figure 3c shows the histogram of duration, revealing that ~96% of observed events last between 20 seconds and 4 minutes, with an additional outlier at 17 minutes. This distribution is comparable to observations at Saturn (Azari et al., 2018), which showed interchange event durations ranging from 2 to 34 minutes, with most lasting less than 10 minutes. It is also consistent with recent observations at Jupiter, which indicated events on the order of one minute with temporal spacings of ~15-40 minutes between different events (Kurth et al., 2023). The corresponding *M*-shell width is typically small, with $|\boldsymbol{\Delta} M|<0.05$, constituting 78% of events (Figure 3d), while $|\boldsymbol{\Delta} M|$ can reach up to 0.6 for the longest events.

3.4 Multi-Event analysis

A multi-event analysis of interchange events associated with plasma waves is shown in Figure 4, sorted by increasing *M*-shell from top to bottom. The columns, labeled as (1) Z-mode, (2) whistler-mode, and (3) ECH, are organized by plasma wave association. The solid (dotted) vertical magenta line indicates the start (end) of each interchange event.

Z-mode waves (Figures 4.1a-e) are observed within $f_{L=0}$ (black) and f_{pe} (red). The plasma frequency is estimated from $f_{L=0}$ and f_{ce} through $\boldsymbol{f_{pe}=\sqrt{f_{L=0}(f_{L=0}+f_{ce})}}$ (Gurnett & Bhattacharjee, 2005), where f_{ce} is depicted with the solid white line. Each of these Z-mode waves is expected to be left-hand circularly polarized or a fast mode. The average frequency bandwidth of all observed Z-mode waves is ~0.27 f_{ce} for events at M<10, broader than other observed plasma waves near the same frequency.

The middle column shows interchange events in association with whistler-mode waves. Narrow-band chorus waves, either upper or lower band, are observed between the marked lines of $0.5f_{ce}$ (yellow) and f_{ce} (white) or below $0.5f_{ce}$, respectively. The average bandwidth of the 13 observed whistler-mode chorus events (8 not shown) is ~$0.22f_{ce}$. It is interesting to note that three whistler-mode associated events are also linked with ECH waves (Figures 4.2a-b).

The final column shows interchange events associated with ECH waves, with f_{ce} and $2f_{ce}$ indicated by the solid and dashed white lines. The first harmonic is intensified in each of these events, with an average peak intensity of 4.6×10^{-6} V/m during all observed events. Some events exhibit an intensification at the 2nd and/or 3rd harmonics with varying durations in wave intensification, possibly owing to modified particle distributions during different periods of the event.

4 Summary and Conclusions

Using wave and particle data from the Juno satellite spanning 2016 to 2023, we conducted a statistical survey of interchange events across a vast region of Jupiter's magnetosphere. The main findings are summarized below.

(1) Interchange events can extend to magnetic latitudes of ~40° and *M*-shells ranging from 6 to ~26, with a peak occurrence rate at M~17. While the magnetic local time coverage of Juno measurements from low to middle magnetic latitudes is limited, statistical results reveal that interchange events occur over the entire nightside.

(2) During interchange events, various types of plasma waves are intensified, including Z-mode, whistler-mode, and ECH waves. Z-mode wave-associated interchange events are observed in the mid latitude range (MLat~17.1°-42°) across *M*-shells of 6.6-25.7. In contrast, whistler-mode wave-associated events tend to occur near the equator (MLat~-15.8°-17°) across *M*-shells of 8.7-22.4. ECH wave-associated events are observed near the equatorial plane (MLat~-3.8°-15.3°) across *M*-shells of 8.7-17.3.

(3) The duration of interchange events measured by the Juno satellite is predominantly less than 4 minutes, with the longest extending up to 17 minutes. Correspondingly, the M-shell width ranges from 0.01 to 0.6, with the majority of interchange events having $|\Delta M|<0.05$.

(4) Each of these events indicates inward radial transport, characterized by a rapid increase (decrease) in magnetic field strength at the onset (end), a rapid increase in hot electron flux (1-100s of keV), a decrease in low-energy electron flux (<~100 eV), and a decrease in total electron number density in association with plasma waves.

It is important to note that our statistical survey includes only fresh interchange events characterized by abrupt changes in magnetic field intensity. Following the occurrence of these fresh interchange events, the particles within the interchange flux tube undergo magnetic and electric drift, leading to further evolution within the Jovian magnetosphere. Additionally, it may be valuable to examine the electron flux at different energies with respect to pitch angle to determine if trapping occurs at higher pitch angles within these flux tubes (Yin et al., 2023).

However, there has been no clear evidence of this phenomenon occurring for electrons in this study thus far. Moreover, it may be worthwhile to evaluate the characteristics of protons and heavy ions during these events, as shown at Saturn (Thomsen et al., 2014).

Nonetheless, our analysis of the interchange instability and its association with electrons and plasma waves reveals the primary locations of interchange events, the characteristics of electrons and plasma waves, as well as the duration and spatial extent of these events. These findings advance our understanding of interchange instability and its influence on electron transport and plasma wave generation in the Jovian magnetosphere, as well as in other magnetized planets within and beyond our solar system.

Acknowledgments

The research at Boston University is supported by the NASA grant 80NSSC20K0557, Subcontract Q99064JAR under NASA Prime contract NNM06AA75C, and NSF grant AGS-2402179. AD would like to acknowledge the NASA FINESST grant 80NSSC23K1641. QM would like to acknowledge the NASA grants 80NSSC20K0196, and 80NSSC24K0572, and the NSF grant AGS-2225445. The work at UCLA was supported by the NASA subcontract 699046X under prime contract ZZM06AA75C. The research at the University of Iowa is supported by NASA through Contract 699041X with the Southwest Research Institute. WSK acknowledges the use of the Space Physics Data Repository at the University of Iowa supported by the Roy J. Carver Charitable Trust.

Data Availability Statement

We acknowledge the Juno data, including JEDI at https://doi.org/10.17189/1519713 (Mauk et al., 2022), JADE at https://doi.org/10.17189/1519715 (Allegrini et al., 2022), Waves at https://doi.org/10.17189/1520498 (Kurth & Piker, 2022a, 2022b), and Magnetometer at https://doi.org/10.17189/1519711 (Connerney, 2022). We also thank the use of Jovian magnetic field model from Laboratory for Atmospheric and Space Physics (LASP) at University of Colorado Boulder (https://lasp.colorado.edu/home/mop/missions/juno/community-code/). The time intervals, location of events, duration, and spatial extent of all observed events can be found at https://doi.org/10.6084/m9.figshare.25452559.v1
The time intervals, location of events, duration, and spatial extent of all observed events can be found at https://doi.org/10.6084/m9.figshare.25452559.v1 (Daly, 2024).

References

Allegrini, F., Wilson, R.J., Ebert, R.W., Loeffler, C. (2022), JUNO J/SW JOVIAN AURORAL DISTRIBUTION CALIBRATED V1.0, JNO-J/SW-JAD-3-CALIBRATED-V1.0 [Dataset], NASA Planetary Data System, https://doi.org/10.17189/1519715.

André, N., M. K. Dougherty, C. T. Russell, J. S. Leisner, and K. K. Khurana (2005), Dynamics of the Saturnian inner magnetosphere: First inferences from the Cassini magnetometers about small-scale plasma transport in the magnetosphere, *Geophys. Res. Lett.*, 32, L14S06, doi:10.1029/2005GL022643.

André, N., et al. (2007), Magnetic signatures of plasma-depleted flux tubes in the Saturnian inner magnetosphere, *Geophys. Res. Lett.*, 34, L14108, doi:10.1029/2007GL030374.

Ashour-Abdalla, M., and C. F. Kennel (1978), Multi-harmonic electron cyclotron instabilities, *Geophys. Res. Lett.*, 5(8), 711–714, doi:10.1029/GL005i008p00711.

Azari, A. R., Liemohn, M. W., Jia, X., Thomsen, M. F., Mitchell, D. G., Sergis, N., et al. (2018). Interchange injections at Saturn: Statistical survey of energetic H^+ sudden flux intensifications. *Journal of Geophysical Research: Space Physics*, 123, 4692–4711. https://doi.org/10.1029/2018JA025391

Azari, A. (2020). A Data-Driven Understanding of Plasma Transport in Saturn's Magnetic Environment, (Doctoral dissertation). Retrieved from Deep Blue. (https://hdl.handle.net/2027.42/155251). Ann Arbor, MI: University of Michigan.

Bhattacharya, B., Thorne, R. M., Williams, D. J., Khurana, K. K., & Gurnett, D. A. (2005). Diffuse auroral precipitation in the Jovian upper atmosphere and magnetospheric electron flux variability. *Icarus*, 178, 406-416. https://doi.org/10.1016/j.icarus.2005.06.013

Bolton, S. J., Thorne, R. M., Gurnett, D. A., Kurth, W. S., & Williams, D. J. (1997). Enhanced whistler-mode emissions: Signatures of interchange motion in the Io torus. *Geophysical Research Letters*, 24(17), 2123–2126. https://doi.org/10.1029/97GL02020

Bolton, S. J. (2010). The Juno mission. *Proceedings of the International Astronomical Union*, 6(S269), 100. https://doi.org/10.1017/S1743921310007313

Burch, J. L., Goldstein, J., Hill, T. W., Young, D. T., Crary, F. J., Coates, A. J., André, N., Kurth, W. S., and Sittler, E. C. (2005), Properties of local plasma injections in Saturn's magnetosphere, *Geophys. Res. Lett.*, 32, L14S02, https://doi.org/10.1029/2005GL022611

Connerney, J.E.P., Benn, M., Bjarno, J.B. *et al.* The Juno Magnetic Field Investigation. *Space Sci Rev* **213,** 39–138 (2017). https://doi.org/10.1007/s11214-017-0334-z

Connerney, J.E.P. (2022), Juno MAG CALIBRATED DATA J V1.0, JNO-J-3-FGM-CAL-V1.0 [Dataset], NASA Planetary Data System. https://doi.org/10.17189/1519711

Chen, Y., Hill, T. W., Rymer, A. M., & Wilson, R. J. (2010). Rate of radial transport of plasma in Saturn's inner magnetosphere. *Journal of Geophysical Research*, **115**, A10211. https://doi.org/10.1029/2010JA015412

Daly, A., Li, W., Ma, Q., Shen, X.-C., Yoon, P. H., Menietti, J. D., et al. (2023). Plasma wave and particle dynamics during interchange events in the Jovian magnetosphere using Juno observations. *Geophysical Research Letters*, 50, e2023GL103894. https://doi.org/10.1029/2023GL103894

Daly, Alec (2024). Statistical Survey of Interchange Events in the Jovian Magnetosphere Using Juno observations. [Dataset]. https://doi.org/10.6084/m9.figshare.25452559.v1

Dougherty, L. P., Bodisch, K. M., and Bagenal, F. (2017), Survey of Voyager plasma science ions at Jupiter: 2. Heavy ions, *J. Geophys. Res. Space Physics*, 122, 8257– 8276, https://doi.org/10.1002/2017JA024053

Dumont, M., Grodent, D., Radioti, A., Bonfond, B., & Gérard, J.-C. (2014). Jupiter's equatorward auroral features: Possible signatures of magnetospheric injections. *Journal*

of Geophysical Research: Space Physics, **119**(12), 10068–10077. https://doi.org/10.1002/2014JA020527
Feng, E., Zhang, B., Yao, Z., Delamere, P. A., Zheng, Z., Dunn, W. R., & Ye, S.-Y. (2023). Variation of the Jovian magnetopause under constant solar wind conditions: Significance of magnetodisc dynamics. *Geophysical Research Letters*, 50, e2023GL104046. https://doi.org/10.1029/2023GL104046
Gurnett, D. A., & Bhattacharjee, A. (2005). *Introduction to Plasma Physics* (p. 97). Cambridge University Press. https://doi.org/10.1017/CBO9780511809125
Hill, T. W., Rymer, A. M., Burch, J. L., Crary, F. J., Young, D. T., Thomsen, M. F., Delapp, D., André, N., Coates, A. J., and Lewis, G. R. (2005), Evidence for rotationally driven plasma transport in Saturn's magnetosphere, *Geophys. Res. Lett.*, 32, L14S10, https://doi.org/10.1029/2005GL022620
Horne, R. B., & Thorne, R. M. (1998). Potential waves for relativistic electron scattering and stochastic acceleration during magnetic storms. *Geophysical Research Letters*, **25**(15), 3011–3014. https://doi.org/10.1029/98GL01002
Horne, R. B., Thorne, R. M., Meredith, N. P., and Anderson, R. R. (2003). Diffuse auroral electron scattering by electron cyclotron harmonic and whistler mode waves during an isolated substorm. *J. Geophys. Res.* 108 (A7), 1290. doi:10.1029/2002JA009736
Hospodarsky, G. B., Sigsbee, K., Leisner, J. S., Menietti, J. D., Kurth, W. S., Gurnett, D. A., Kletzing, C. A., & Santolí, K, O. (2012). In D. Summers, I. R. Mann, D. N. Baker, & M. Schulz (Eds.), *Plasma wave observations at Earth, Jupiter, and Saturn. In dynamics of the Earth's radiation belts and inner magnetosphere*, Washington DC: American Geophysical Union. https://doi.org/10.1029/2012GM001342
Joseph, J., Jaynes., A. N., Kurth, W. S., Menietti, J. D., Connerney, J. E. P., Bolton, S. J., (2023) Electron cyclotron harmonic waves in Jovian magnetosphere as seen by Juno. *Frontiers in Astronomy and Space Sciences.,* 10, https://doi.org/10.3389/fspas.2023.1274760
Kennel, C., "Low-Frequency Whistler Mode", The Physics of Fluids, 9, 2190-2202 (1966) https://doi.org/10.1063/1.1761588
Kennel, C. F., Scarf, F. L., Fredricks, R. W., McGehee, J. H., and Coroniti, F. V. (1970). VLF electric field observations in the magnetosphere. *J. Geophys. Res.* 75 (31), 6136–6152. doi:10.1029/JA075i031p06136
Kivelson, M. G., K. K. Khurana, C. T. Russell, and R. J. Walker (1997), Intermittent short-duration magnetic field anomalies in the IO torus: Evidence for plasma interchange?, *Geophysical Research Letters*, *24*(17), 2127–2130, https://doi.org/10.1029/97GL02202
Kurth, W. S., Hospodarsky, G. B., Kirchner, D. L., Mokrzycki, B. T., Averkamp, T. F., Robison, W. T., et al. (2017). The Juno Waves investigation. *Space Science Reviews*, **213**(1-4), 347–392. https://doi.org/10.1007/s11214-017-0396-y
Kurth, W. S., & Piker, C. W. (2022a). JUNO E/J/S/SS WAVES CALIBRATED BURST FULL RESOLUTION V2.0, JNO-E/J/SS-WAV-3-CDR-BSTFULL-V2.0 [Dataset]. NASA Planetary Data System. https://doi.org/10.17189/1522461

Kurth, W. S., & Piker, C. W. (2022b). JUNO E/J/S/SS WAVES CALIBRATED SURVEY FULL RESOLUTION V2.0, JNO-E/J/SS-WAV-3-CDR-SRVFULL-V2.0 [Dataset]. NASA Planetary Data System. https://doi.org/10.17189/1520498

Kurth, W. S., Hospodarsky, G. B., Faden, J. B, Sulaiman, A. H., Mauk, B. H., Clark, G., Allegrini, F., Connerney, J. E. P., and Bolton, S. J. (2023), Evidence of fresh interchange injections related to the interchange instability in the Io torus. https://doi.org/10.25546/103104

Lai, H. R., Russell, C. T., Jia, Y. D., Wei, H. Y., & Dougherty, M. K. (2016). Transport of magnetic flux and mass in Saturn's inner magnetosphere. *Journal of Geophysical Research: Space Physics*, **121**, 3050–3057. https://doi.org/10.1002/2016JA022436

Li, W., Thorne, R. M., Meredith, N. P., Horne, R. B., Bortnik, J., Shprits, Y. Y., and Ni, B. (2008), Evaluation of whistler mode chorus amplification during an injection event observed on CRRES, J. Geophys. Res., 113, A09210, doi:10.1029/2008JA013129.

Li, W., Shen, X.-C., Menietti, J. D., Ma, Q., Zhang, X.-J., Kurth, W. S., & Hospodarsky, G. B. (2020). Global distribution of whistler mode waves in Jovian inner magnetosphere. *Geophysical Research Letters*, 47, e2020GL088198. https://doi.org/10.1029/2020GL088198

Li, W., Ma, Q., Shen, X.-C., Zhang, X.-J., Mauk, B. H., Clark, G., et al. (2021). Quantification of diffuse auroral electron precipitation driven by whistler mode waves at Jupiter. Geophysical Research Letters, 48, e2021GL095457. https://doi.org/10.1029/2021GL095457

Li, W., Ma, Q., Shen, X.-C., Zhang, X.-J., Mauk, B. H., Clark, G., et al. (2023). Driver of energetic electron precipitation in the vicinity of Ganymede. Geophysical Research Letters, 50, e2022GL101555.

Mauk, B. H., Haggerty, D. K., Jaskulek, S. E. *et al.* The Jupiter Energetic Particle Detector Instrument (JEDI) Investigation for the Juno Mission. *Space Sci Rev* **213,** 289–346 (2017). https://doi.org/10.1007/s11214-013-0025-3

Mauk, B. (APL), JEDI CALIBRATED (CDR) DATA JNO J JED 3 CDR V1.0 [Dataset], NASA Planetary Data System, 2022, https://doi.org/10.17189/1519713.

McComas, D. J., Alexander, N., Allegrini, F., et al. (2017). The Jovian Auroral Distributions Experiment (JADE) on the Juno Mission to Jupiter. *Space Science Reviews*, *213*(1-4), 547-643. https://doi.org/10.1007/s11214-013-9990-9

Menietti, J. D., Averkamp, T. F., Kurth, W. S., Imai, M., Faden, J. B., Hospodarsky, G. B., et al. (2021). Analysis of whistler-mode and Z-mode emission in the Juno primary mission. Journal of Geophysical Research: Space Physics, 126, e2021JA029885. https://doi.org/10.1029/2021JA029885

Menietti, J. D., Averkamp, T. F., Kurth, W. S., Faden, J. B., & Bolton, S. J. (2023). Survey and analysis of whistler- and Z-mode emission in the Juno extended mission. *Journal of Geophysical Research: Space Physics*, 128, e2023JA032037. https://doi.org/10.1029/2023JA032037

Mitchell, D.G., Brandt, P.C., Carbary, J.F., Kurth, W.S., Krimigis, S.M., Paranicas, C., Krupp, N., Hamilton, D.C., Mauk, B.H., Hospodarsky, G.B., Dougherty, M.K. and Pryor, W.R. (2015). Injection, Interchange, and Reconnection. In Magnetotails in the Solar System (eds A. Keiling, C.M. Jackman and P.A. Delamere). https://doi.org/10.1002/9781118842324.ch19

Ni, B., Liang, J., Thorne, R. M., Angelopoulos, V., Horne, R. B., Kubyshkina, M., et al. (2012). Efficient diffuse auroral electron scattering by electrostatic electron cyclotron harmonic waves in the outer magnetosphere: a detailed case study. *J. Geophys. Res.* 117, A01218. doi:10.1029/2011JA017095

Paranicas, C., Thomsen, M. F., Kollmann, P., Azari, A. R., Bader, A., Badman, S. V., et al. (2020). Inflow speed analysis of interchange injections in Saturn's magnetosphere. *Journal of Geophysical Research: Space Physics*, 125, e2020JA028299. https://doi.org/10.1029/2020JA028299

Rymer, A. M. & Mauk, B. H. & Hill, T. W. & André, Nicolas & Mitchell, Donald & Paranicas, C. & Young, D. & Smith, H.T. & Persoon, A.M. & Menietti, J. D. & Hospodarsky, George & Coates, Andrew & Dougherty, M. K. (2009). Cassini evidence of rapid interchange transport at Saturn. Planetary and Space Science. 57. 1779-1784. https://doi.org/10.1016/j.pss.2009.04.010

Southwood, D. J., and M. G. Kivelson (1987), Magnetospheric interchange instability, *J. Geophys. Res.*, **92**(A1), 109–116, https://doi.org/10.1029/JA092iA01p00109

Southwood, D. J., and M. G. Kivelson (1989), Magnetospheric interchange motions, *J. Geophys. Res.*, 94(A1), 299–308, https://doi.org/10.1029/JA094iA01p00299

Tanaka, T., Ebihara, Y., Watanabe, M., Fujita, S., & Kataoka, R. (2023). Radial transport of Io plasma from the inner magnetosphere to the tail. *Journal of Geophysical Research: Space Physics*, 128, e2022JA030891. https://doi.org/10.1029/2022JA030891

Thomsen, M. F. (2013), Saturn's magnetospheric dynamics, *Geophys. Res. Lett.*, 40, 5337–5344, https://doi.org/10.1002/2013GL057967

Thomsen, M. F., Reisenfeld, D. B., Wilson, R. J. et al. (2014), Ion composition in interchange injection events in Saturn's magnetosphere, *J. Geophys. Res. Space Physics*, 119, 9761–9772, https://doi.org/10.1002/2014JA020489

Thorne, R. M., T. P. Armstrong, S. Stone, D. J. Williams, R. W. McEntire, S. J. Bolton, D. A. Gurnett, and M. G. Kivelson (1997), Galileo evidence for rapid interchange transport in the Io Torus, *Geophysical Research Letters*, *24*(17), 2131–2134, https://doi.org/10.1029/97gl01788

Tilley, M. A., and Harnett, E. M., and Winglee, R. M. (2016). Extrasolar Giant Magnetospheric Response to Steady-state Stellar Wind Pressure at 10, 5, 1, and 0.2 au, *Astrophys. J.*, 827(1), 77, https://doi.org/10.3847/0004-637x/827/1/77

Wu, C. S., and L. C. Lee (1979), A theory of terrestrial kilometric radiation, *Astrophys. J.*, **230**, 621, https://doi.org/10.1086/157120

Xiao, F., Thorne, R. M., Gurnett, D. A., and Williams, D. J. (2003), Whistler-mode excitation and electron scattering during an interchange event near Io, *Geophys. Res. Lett.*, 30, 1749, https://doi.org/10.1029/2003GL017123

Yin, Z.-F., Sun, Y.-X., Zhou, X.-Z., Pan, D.-X., Yao, Z.-H., Yue, C., et al. (2023). Trapped and leaking energetic particles in injection flux tubes of Saturn's magnetosphere. *Geophysical Research Letters*, 50, e2023GL105687. https://doi.org/10.1029/2023GL105687

Yoon, P. H., Weatherwax, A. T., and Rosenberg, T. J. (1998), On the generation of auroral radio emissions at harmonics of the lower ionospheric electron cyclotron frequency: *X*, *O* and *Z* mode maser calculations, *J. Geophys. Res.*, 103(A3), 4071– 4078, https://doi.org/10.1029/97JA03526

Zhang, X., and Angelopoulos, V. (2014). On the relationship of electrostatic cyclotron harmonic emissions with electron injections and dipolarization fronts. *J. Geophys. Res. Space Phys.* 119, 2536–2549. https://doi.org/10.1002/2013JA019540

Supporting References

Kollmann, P., Paranicas, C., Clark, G., Mauk, B. H., Haggerty, D. K., Rymer, A. M., et al. (2017). A heavy ion and proton radiation belt inside of Jupiter's rings. Geophysical Research Letters, 44(11), 5259–5268. https://doi.org/10.1002/2017GL073730

Rymer, A. M. & Mauk, B. H. & Hill, T. W. & André, Nicolas & Mitchell, Donald & Paranicas, C. & Young, D. & Smith, H.T. & Persoon, A.M. & Menietti, J. D. & Hospodarsky, George & Coates, Andrew & Dougherty, M. K. (2009). Cassini evidence of rapid interchange transport at Saturn. Planetary and Space Science. 57. 1779-1784. https://doi.org/10.1016/j.pss.2009.04.010

Southwood, D. J., and M. G. Kivelson (1987), Magnetospheric interchange instability, *J. Geophys. Res.*, **92**(A1), 109–116, https://doi.org/10.1029/JA092iA01p00109

Figures.

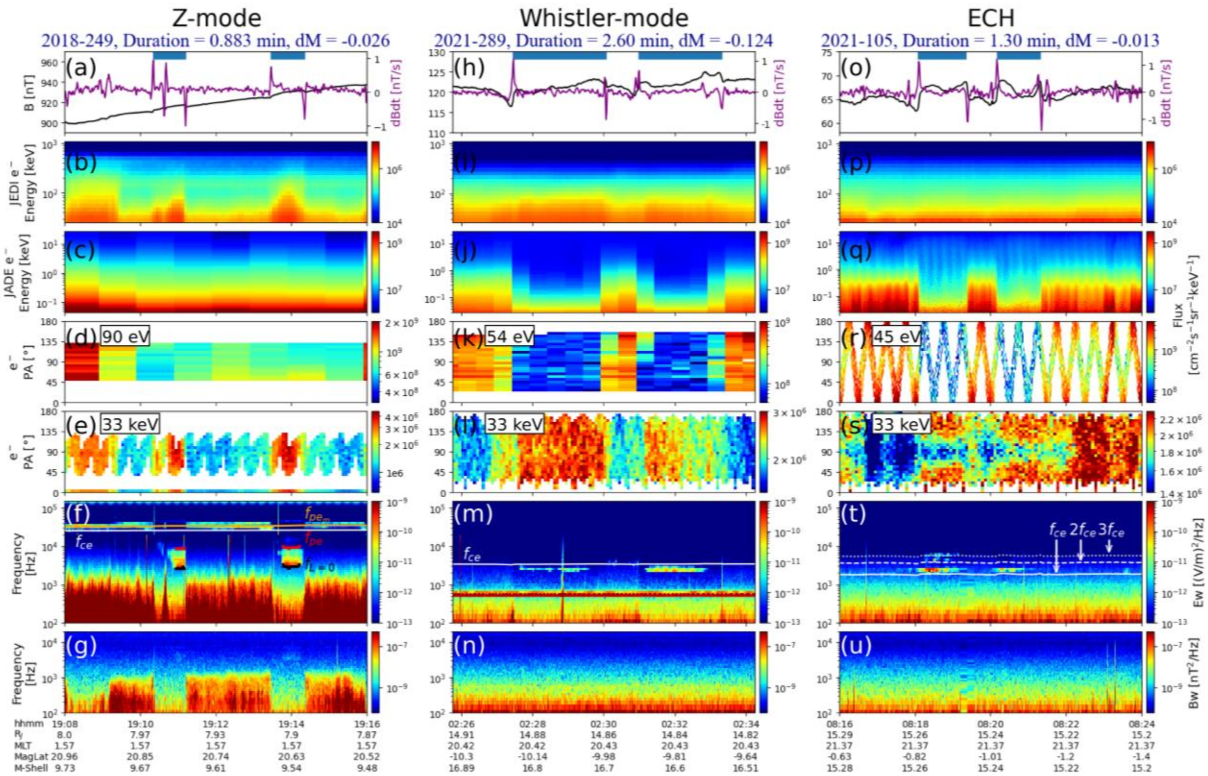

Figure 1. Juno observations of energetic electrons and plasma waves for three interchange events (marked by blue bars), where the associated plasma waves are Z-mode (left), whistler-mode (middle), and ECH waves (right). (a) Magnetic field strength (black) and rate of change (*dB/dt*, purple); (b) Energy spectrogram of electron flux from ~30 keV to ~1 MeV observed by JEDI; (c) Energy spectrogram of electron flux from 100 eV to 30 keV observed by JADE; (d) Pitch angle distribution of electron fluxes at 90 eV and (e) 33 keV; (f) Wave electric spectrogram from 100 Hz-150 kHz, where the solid black line represents $f_{L=0}$, the solid red line is f_{pe}, the solid orange line is the modeled plasma frequency ($f_{pe\ m}$), the white solid line is f_{ce}, and the white dotted and dashed lines are $2f_{ce}$ and $3f_{ce}$.; (g) Wave magnetic spectrogram from 100 Hz-20 kHz. (h)-(n) Similar format to panels (a)-(g) but for the whistler-mode wave event. (o)-(u) Similar format to panels (a)-(g) but for the ECH wave event.

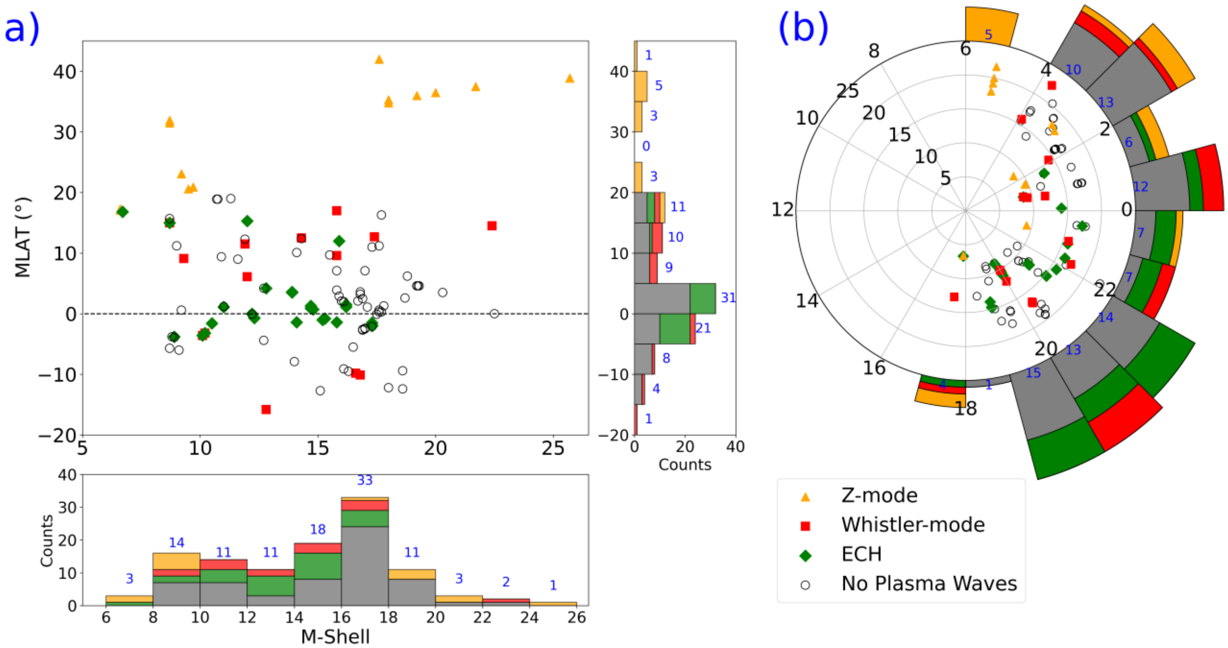

Figure 2. Distribution of observed interchange events from July 2016 to May 2023. (a) Distribution of events in *M*-shell and MLat. Interchange events are sorted by associated plasma waves, with orange triangles representing Z-mode waves, red squares representing whistler-mode waves, green diamonds representing ECH waves, and empty black circles representing no detected plasma waves. The count rate of events is binned by *M*-shell width of 2 and MLat width of 5°. (b) Distribution of events in *M*-shell and MLT, with binned count rate at every MLT hour.

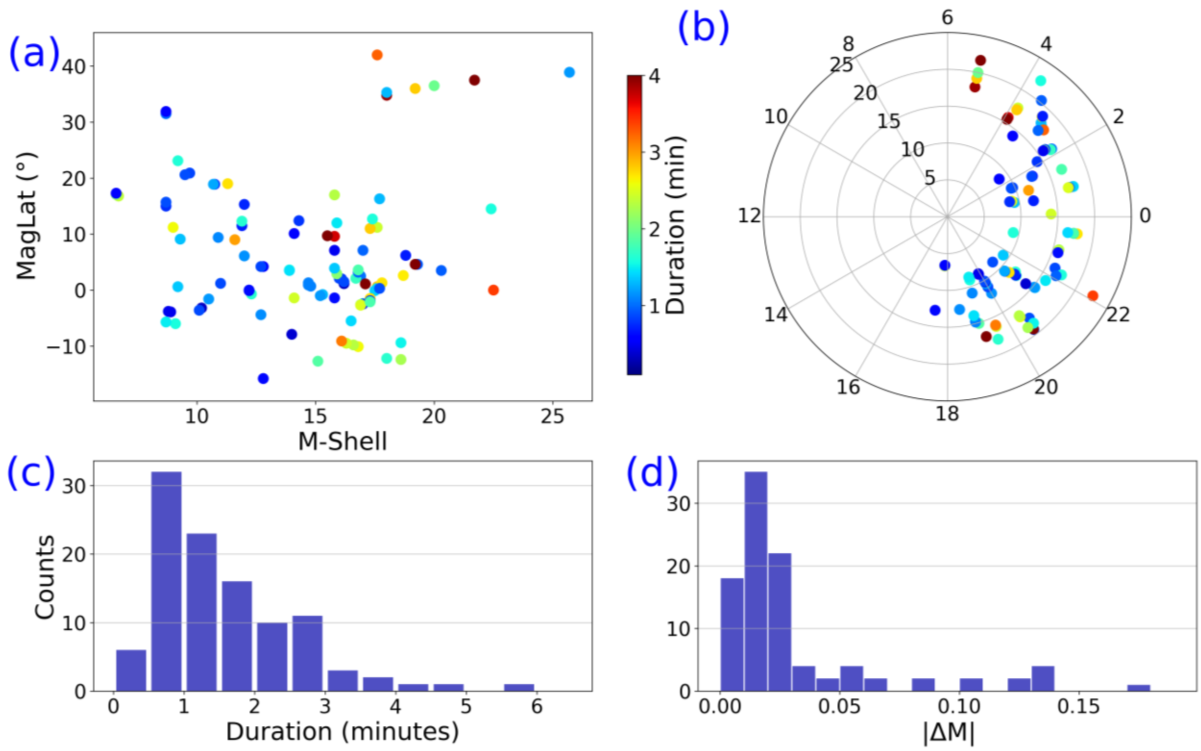

Figure 3. Duration of interchange events in *M*-shell-MLT-MLat coordinates. (a) Duration distribution in *M*-shell and MLat; (b) duration distribution in *M*-shell and MLT; (c) histogram of interchange event duration in minutes, with 11 bins of 30s width ranging from ~20 seconds to 6 minutes, with one outlier near 17 minutes (not shown); (d) similar format to panel (c) but shown for the corresponding change in *M*-shell of the spacecraft during the interchanged flux tube crossing (or the *M*-shell width of the interchange events).

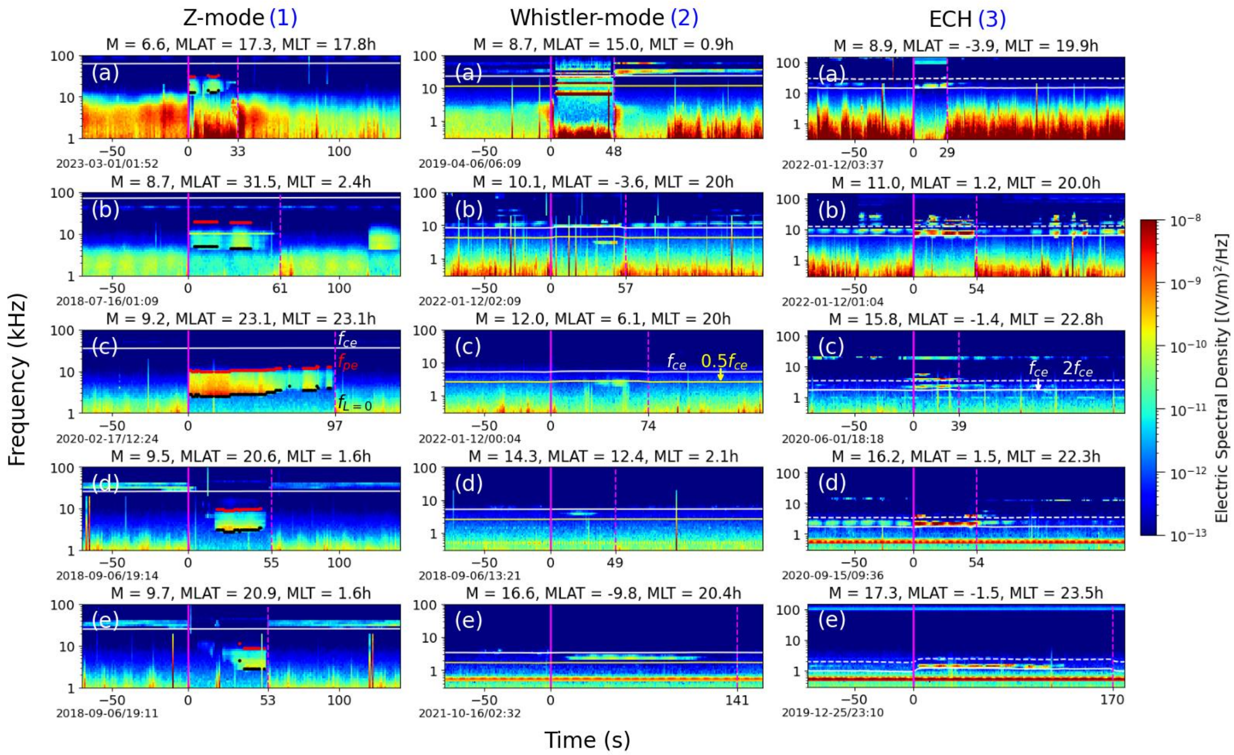

Figure 4. Multi-event analysis of plasma wave electric spectral density during interchange events, categorized by (1) Z-mode, (2) whistler-mode, and (3) ECH waves. Zero epoch time indicates the start (end) of the interchange event, marked by a magenta solid (dashed) vertical line. Events are ordered by increasing M-shell from top to bottom, with information on MLat, MLT, and the date of event start time. (1) Z-mode waves confined between the $f_{L=0}$ (black line) and f_{pe} (red line), with the white line representing f_{ce}. (2) Whistler-mode wave events with the solid yellow line representing $0.5f_{ce}$. (3) ECH wave events with the white dotted line representing $2f_{ce}$.

Figure 1.

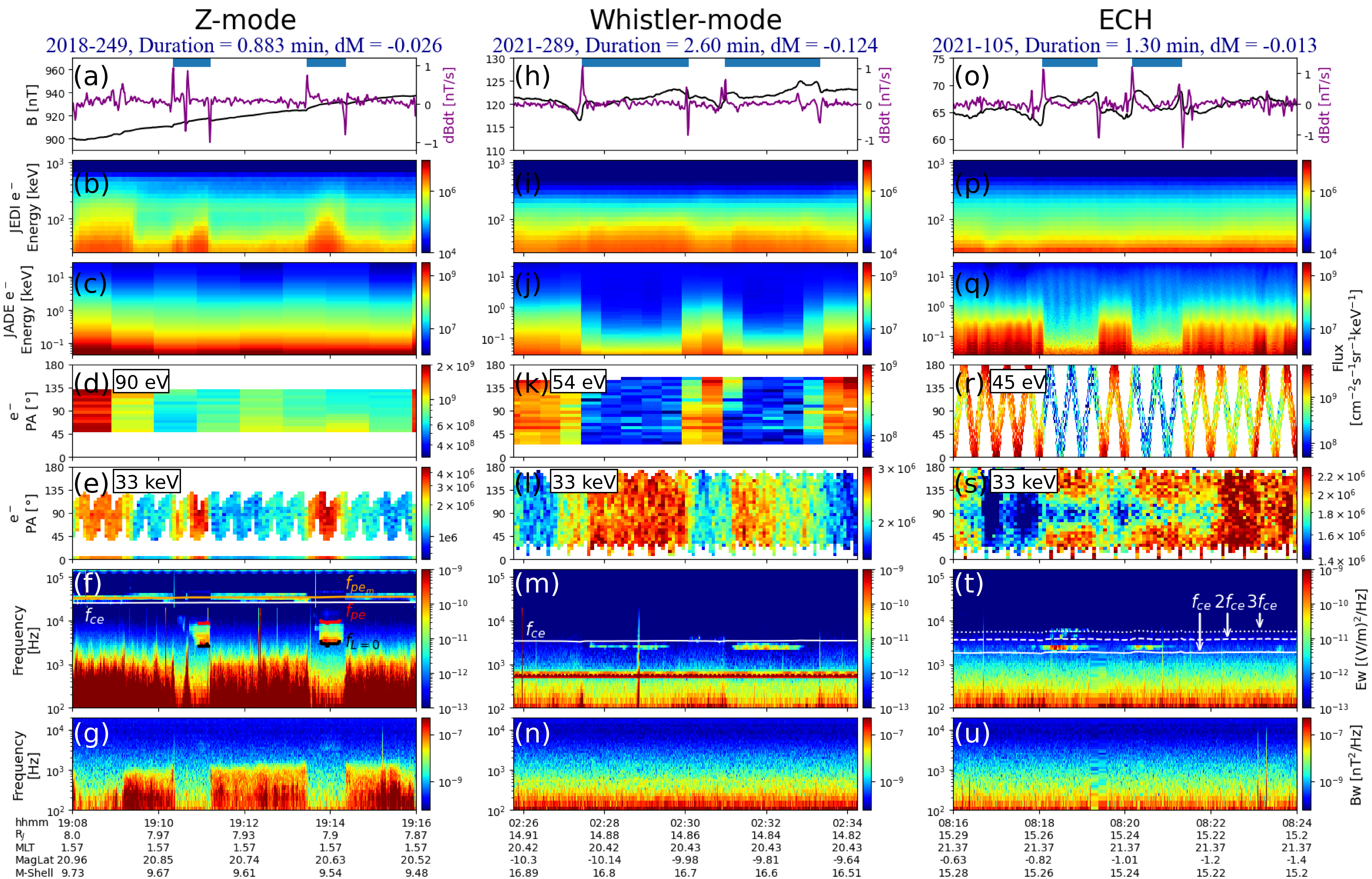

Z-mode
2018-249, Duration = 0.883 min, dM = -0.026
Whistler-mode
2021-289, Duration = 2.60 min, dM = -0.124
ECH
2021-105, Duration = 1.30 min, dM = -0.013
B [nT]
dBdt [nT/s]
JEDI e⁻ Energy [keV]
JADE e⁻ Energy [keV]
e⁻ PA [°]
90 eV
54 eV
45 eV
33 keV
Frequency [Hz]
Flux [cm⁻²s⁻¹sr⁻¹keV⁻¹]
Ew [(V/m)²/Hz]
Bw [nT²/Hz]
f_ce
f_pe_m
f_pe
f_L=0
f_ce 2f_ce 3f_ce
hhmm 19:08 19:10 19:12 19:14 19:16
Rj 8.0 7.97 7.93 7.9 7.87
MLT 1.57 1.57 1.57 1.57 1.57
MagLat 20.96 20.85 20.74 20.63 20.52
M-Shell 9.73 9.67 9.61 9.54 9.48
02:26 02:28 02:30 02:32 02:34
14.91 14.88 14.86 14.84 14.82
20.42 20.42 20.43 20.43 20.43
-10.3 -10.14 -9.98 -9.81 -9.64
16.89 16.8 16.7 16.6 16.51
08:16 08:18 08:20 08:22 08:24
15.29 15.26 15.24 15.22 15.2
21.37 21.37 21.37 21.37 21.37
-0.63 -0.82 -1.01 -1.2 -1.4
15.28 15.26 15.24 15.22 15.2

Figure 2.

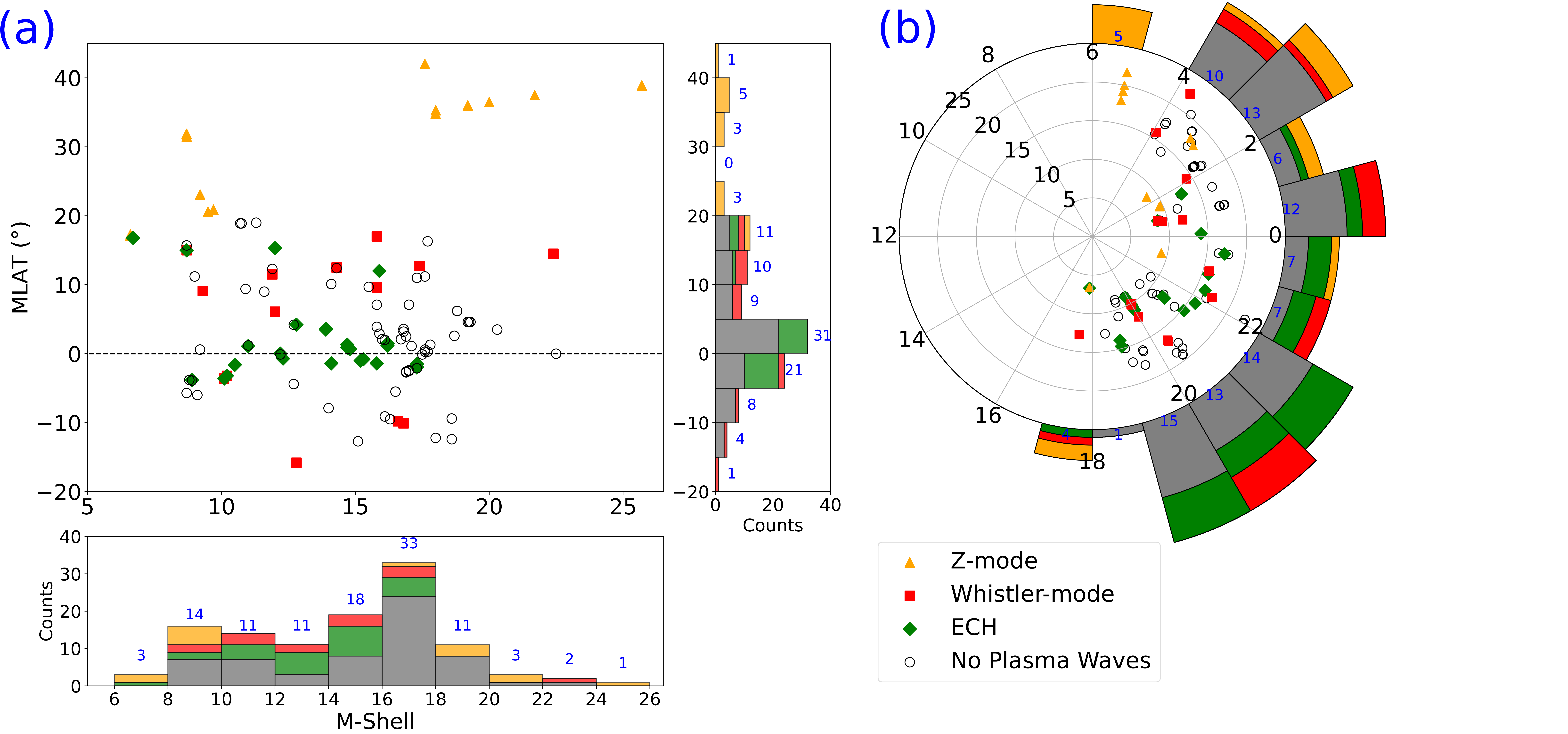

(a)
(b)
MLAT (°)
Counts
M-Shell
Z-mode
Whistler-mode
ECH
No Plasma Waves

Figure 3.

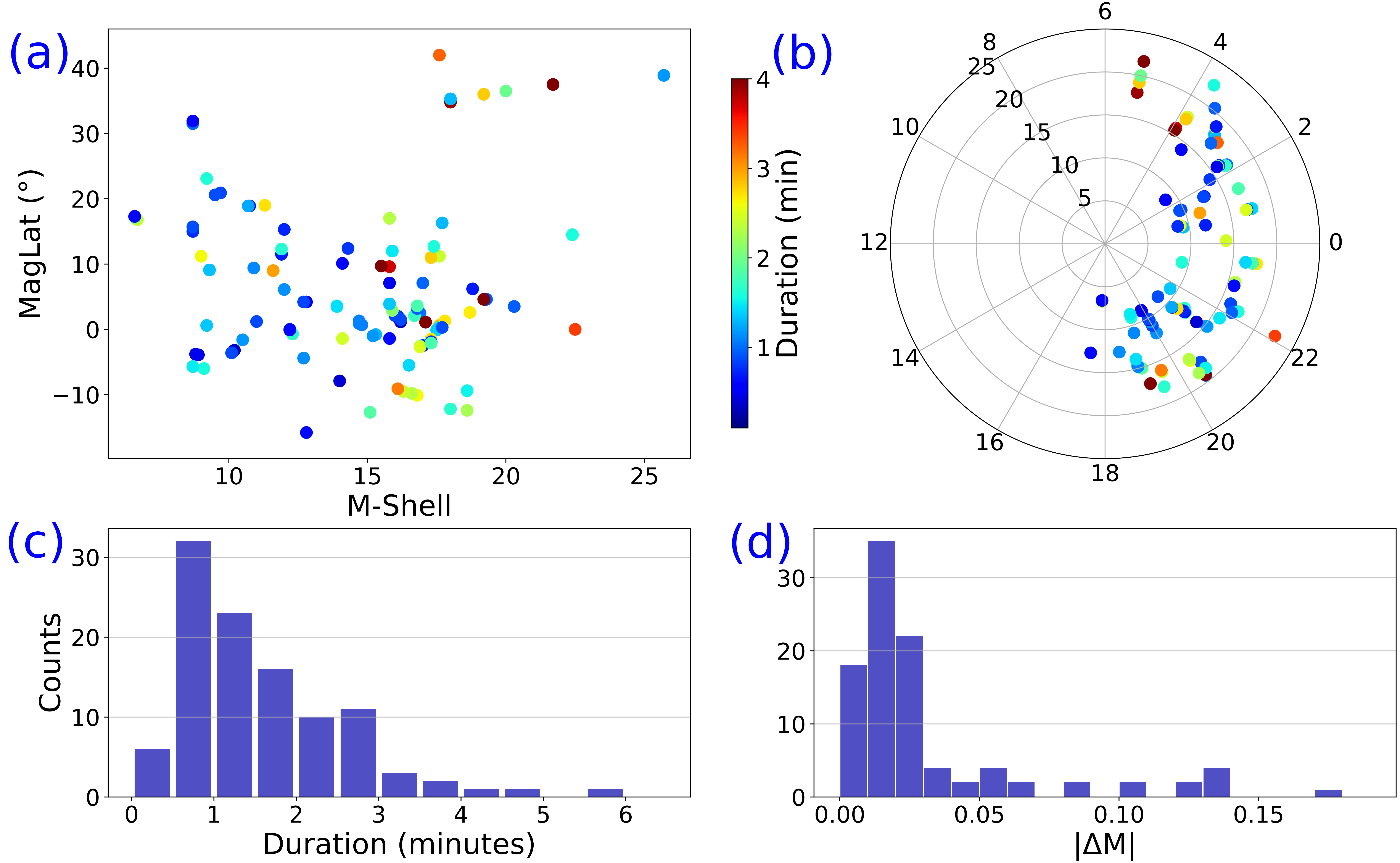

(a)
MagLat (°)
M-Shell
Duration (min)
(b)
(c)
Counts
Duration (minutes)
(d)
|ΔM|

Figure 4.

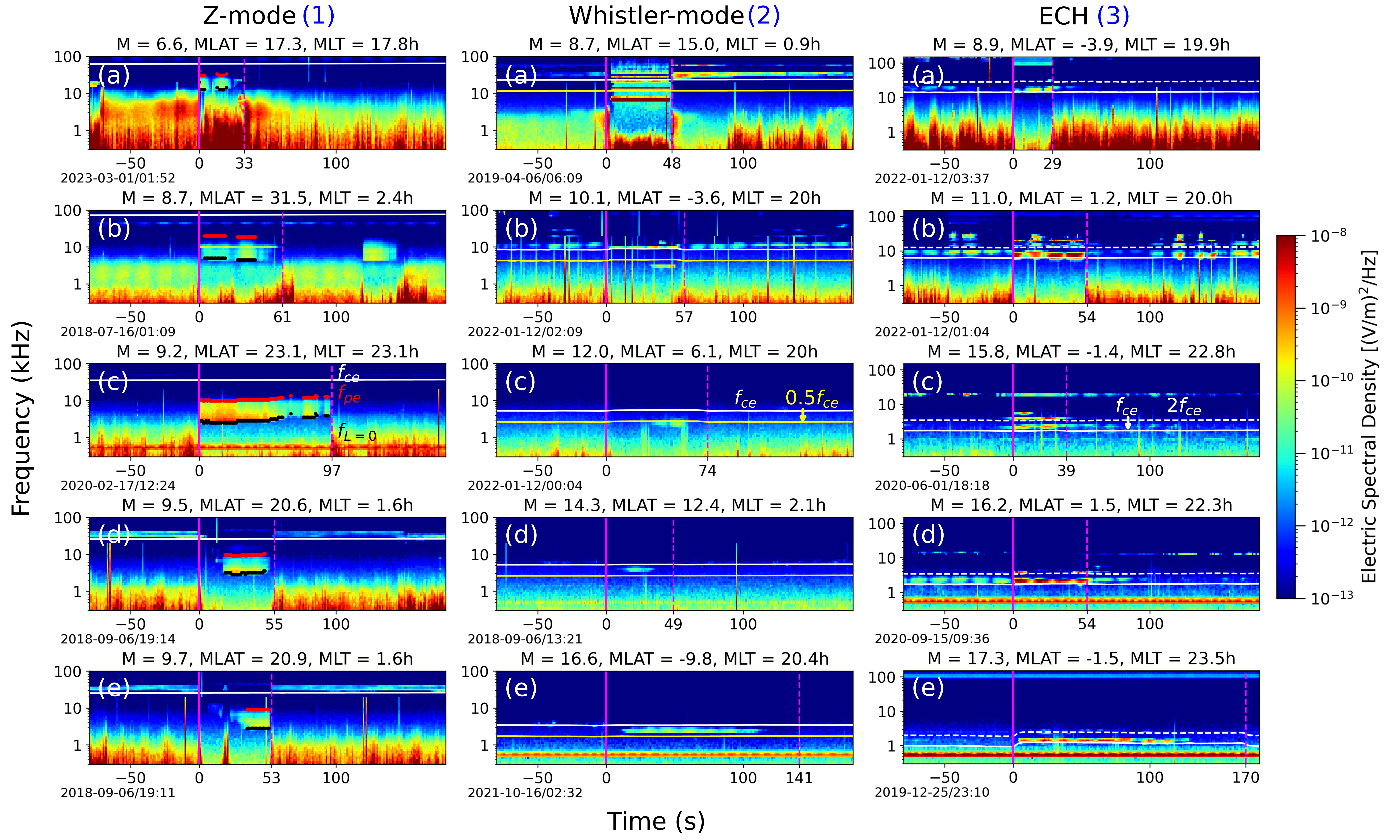

Z-mode (1)
Whistler-mode (2)
ECH (3)
M = 6.6, MLAT = 17.3, MLT = 17.8h
M = 8.7, MLAT = 15.0, MLT = 0.9h
M = 8.9, MLAT = -3.9, MLT = 19.9h
2023-03-01/01:52
2019-04-06/06:09
2022-01-12/03:37
M = 8.7, MLAT = 31.5, MLT = 2.4h
M = 10.1, MLAT = -3.6, MLT = 20h
M = 11.0, MLAT = 1.2, MLT = 20.0h
2018-07-16/01:09
2022-01-12/02:09
2022-01-12/01:04
M = 9.2, MLAT = 23.1, MLT = 23.1h
M = 12.0, MLAT = 6.1, MLT = 20h
M = 15.8, MLAT = -1.4, MLT = 22.8h
f_{ce}
f_{pe}
$f_{L=0}$
$0.5f_{ce}$
$2f_{ce}$
2020-02-17/12:24
2022-01-12/00:04
2020-06-01/18:18
M = 9.5, MLAT = 20.6, MLT = 1.6h
M = 14.3, MLAT = 12.4, MLT = 2.1h
M = 16.2, MLAT = 1.5, MLT = 22.3h
2018-09-06/19:14
2018-09-06/13:21
2020-09-15/09:36
M = 9.7, MLAT = 20.9, MLT = 1.6h
M = 16.6, MLAT = -9.8, MLT = 20.4h
M = 17.3, MLAT = -1.5, MLT = 23.5h
2018-09-06/19:11
2021-10-16/02:32
2019-12-25/23:10
Frequency (kHz)
Time (s)
Electric Spectral Density [(V/m)^2/Hz]